PHYSICAL REVIEW B VOLUME 25, NUMBER 10 15 MAY 1982

Surface shape resonances

Purna C. Das and Joel I. Gersten
Department of Physics, City College of the City University of New York, New York, New York 10031
(Received 24 August 1981; revised manuscript received 29 October 1981)

The system consisting of a hemispheroidal bump protruding from a dielectric half-space possesses surface electromagnetic resonances whose resonant frequencies are a sensitive function of the shape of the bump. The widths of the resonances are determined by couplings to delocalized excitations such as surface plasmons, photons, and by resistive losses due to inelastic electron scattering, in the case of electronic excitations, and surface phonons, photons, and acoustic phonons in the case of ionic lattice excitations.

I. INTRODUCTION

The term "shape resonance" has usually been associated with the field of nuclear physics and refers to the resonance brought about by the shape of the nuclear potential function. In contrast, this article refers to solid-state surface physics and is concerned with resonances which owe their existence to the geometric shape of the surface.

The electrodynamic properties of surfaces with "nontrivial" shapes has been of considerable interest lately. It has been found that the optical properties of molecules in the vicinity of rough surfaces or surfaces deliberately prepared with undulations or "posts" differ markedly from those of isolated molecules or molecules near smooth flat surfaces. Enhanced local optical fields are believed to be responsible for a large part of the surface-enhanced Raman scattering (SERS).[1] In addition, observation of fluorescence anomalies[2] and even nonlinear phenomena at weak field strengths[3] lend credence to the importance of enhanced local fields. In this paper we will argue that the origin of the strong local field is due to the excitation of a surface electromagnetic shape resonance and our goal will be to study its properties.

The model to be considered consists of a dielectric half-space with a hemispheroidal protrusion. The dielectric constant of the solid is $\epsilon(\omega)$ and is, in general, complex. Let the semiaxis of the protrusion perpendicular to the plane be denoted by a and the semiaxis in the surface plane (radius) be denoted by b. The case $a=b$ corresponds to a hemispherical protrusion and has already been studied by Berreman,[4] and more recently by Ruppin,[5] in the context of SERS. It is assumed that a and b are sufficiently small compared with the wavelength of light that retardation effects are weak and may be taken into account perturbatively.

In the zeroth order of approximation, where retardation effects are completely neglected, the excitation spectrum consists of a continuum of propagating states and a discrete set of localized states. The low-lying discrete states are characterized by having large field amplitudes in the neighborhood of the surface protrusion. The higher-lying discrete states have significant field amplitude over a localized region of the surface around the bump. The discrete states are localized in that the field amplitudes fall off to zero rapidly as the region near the bump is left.

If we are talking about the electronic states of a metal the discrete states are the "bump" plasma oscillations. For an insulator or semiconductor whose ions are vibrating the discrete states are the "bump" vibrations of the lattice.

In the case of electronic excitations the continuum states of interest are of three types: the surface plasmons, the photons, and the resistive-loss spectrum, consisting of phonons at low-momentum transfer and, in addition, electron-hole pairs at high-momentum transfers. A consideration of these excitations has already been given in the context of the SERS problem.[6] It is important, however, to emphasize that in this paper we are considering the bare (but rough) surface without any molecular adsorbate.

In the case of ionic excitation of an insulator or semiconductor the continuum states of interest consist of surface phonons, photons, and other bulk phonons which may be excited through anharmonic couplings. Naturally it is possible to envisage more complicated situations where the

phonons and plasmons must be jointly considered.

For clarity's sake let us focus our attention on the electronic excitation case. Let us further restrict our attention now to the case of surface plasmons. At large wave vector parallel to the surface $\vec{k}_{||}$, the energy wave-vector dispersion curve of the plasmon is basically flat (except for effects due to nonlocality at very large $\vec{k}_{||}$). At small wave vector, retardation effects set in and the dispersion curve falls towards zero. The energies of the discrete states lie below the energy of the surface plasmon in the large $\vec{k}_{||}$ region. In the small $\vec{k}_{||}$ domain, however, they will be degenerate with some plasmon states. One is then faced with a situation in which a discrete localized state is degenerate with a continuum of delocalized states. The electric dipole of the bump couples with the electric field of the extended surface plasmon. The localized state gets transformed into a resonance and develops a finite lifetime because of the mutual coupling. This is the prototype for the origin of a resonance.

It should, perhaps, be pointed out that the coupling to resistive losses causes a decay of even a localized state. It basically provides a decay channel whereby the energy of the localized state can go into Ohmic heating of the dielectric. Such energy deposition is relatively short ranged and not severely sensitive to the surface shape. It differs from decay into surface plasmons or photons, which represent long-range energy deposition mechanisms. The plasmon or photon may travel long distances before an absorption process occurs. (In the case of the photon, the light may even be detected). Thus, although all three energy deposition processes will be studied, it is the latter two that are of primary interest.

The paper is organized as follows. In Sec. II we derive expressions for the resonance frequency as a function of the shape of the bump. Section III contains calculations of the decay rates into photons and surface plasmons. Finally in Sec. IV we present our results and discussion.

II. RESONANCE FREQUENCIES

To lowest order, the frequencies of the surface shape resonances are determined by neglecting retardation effects and solving Laplace's equation subject to the appropriate boundary conditions. This will be accomplished by working in prolate spheroidal coordinates (ξ,η,ϕ). The geometry of the bump is determined by the height of the bump above the surface, a, and the radius of the bump in the plane of the surface, b. In place of a and b it is more convenient to introduce a scale-size parameter $f=(a^2-b^2)^{1/2}$ and a shape parameter $\xi_0=a/f$. For the case where $a<b$, an appropriate analytic continuation is implied. Our attention will be limited to the case of axially symmetric modes of excitation, although azimuthally excited modes also exist. For the sake of generality we assume for now that an external field E_0 is applied perpendicular to the surface.

The geometry of the problem is illustrated in Fig. 1. Three regions are depicted: I, II, and III. The potential in these three regions is expandable in terms of Legendre functions of the first and second kind, P_n and Q_n, respectively:

$$\Phi_{\rm I}=\sum_n A_n P_n(\xi)P_n(\eta)\ , \tag{2.1a}$$

$$\Phi_{\rm II}=\sum_n B_n Q_n(\xi)P_n(\eta)-E_0 f P_1(\xi)P_1(\eta)\ , \tag{2.1b}$$

$$\Phi_{\rm III}=\sum_n C_n Q_n(\xi)P_n(\eta)-E_1 f P_1(\xi)P_1(\eta)\ . \tag{2.1c}$$

The coefficients A_n, B_n, C_n, and E_1 are determined by matching Φ at the surfaces and by matching the normal component of the electric displacement vector at the surfaces. The surfaces of interest are defined by $\xi=\xi_0$ for $0<\eta<1$, $\eta=0$ for $\xi_0<\xi<\infty$, and $\xi=\xi_0$ for $-1<\eta<0$. The last surface corresponds to a fiduciary surface in the dielectric, while the former two surfaces correspond to real dielectric-vacuum boundaries. The following equations are obtained:

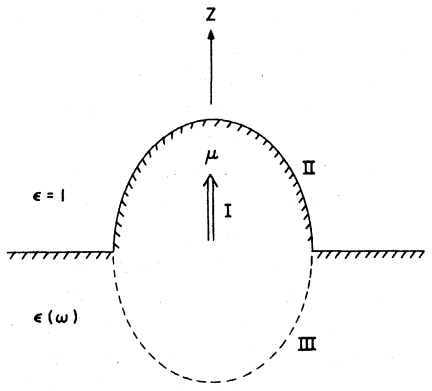

FIG. 1. Schematic diagram of the solid-vacuum interface.

$$\sum_n A_n P_n(\xi_0)P_n(\eta)=\sum_n B_n Q_n(\xi_0)P_n(\eta) - E_0 f \xi_0 P_1(\eta)\,, \tag{2.2a}$$

$$\epsilon\sum_n A_n P_n'(\xi_0)P_n(\eta)=\sum_n B_n Q_n'(\xi_0)P_n(\eta) - E_0 f P_1(\eta)\,, \tag{2.2b}$$

$$\sum_n A_n P_n(\xi_0)P_n(\eta)=\sum_n C_n Q_n(\xi_0)P_n(\eta) - E_1 f P_1(\xi_0)P_1(\eta)\,, \tag{2.2c}$$

$$\sum_n A_n P_n'(\xi_0)P_n(\eta)=\sum_n C_n Q_n'(\xi_0)P_n(\eta) - E_1 f P_1(\eta)\,, \tag{2.2d}$$

$$\sum_n B_n Q_n(\xi)P_n(0)-E_0 f P_1(\xi)P_1(0) = \sum_n C_n Q_n(\xi)P_n(0)-E_1 f P_1(\xi)P_1(0)\,, \tag{2.2e}$$

$$\sum_n B_n Q_n(\xi)P_n'(0)-E_0 f P_1(\xi)P_1'(0) = \epsilon\sum_n C_n Q_n(\xi)P_n'(0)-\epsilon E_1 f P_1(\xi)P_1'(0)\,. \tag{2.2f}$$

Equations (2.2a) and (2.2b) hold for $0<\eta<1$ while (2.2c) and (2.2d) hold for $-1<\eta<0$. Equations (2.2e) and (2.2f) are valid for $\xi>\xi_0$. Equations (2.2a)–(2.2f) may be thought of as generalizations of the corresponding equations derived by Berreman[6] for the case of a hemispherical bump.

The coefficient B_1 is simply related to the electric dipole moment of the system. This is seen by examining the asymptotic potential in region II:

$$\Phi_{\rm II} \underset{\xi\to\infty}{\longrightarrow} B_1 Q_1(\xi)P_1(\eta)-E_0 Z \to \frac{B_1 f^2}{3}\frac{Z}{r^3}-E_0 Z\,, \tag{2.3}$$

in which case we find the dipole to be

$$\mu=\frac{B_1 f^2}{3}\,. \tag{2.4}$$

Let us proceed to obtain expressions for the various expansion coefficients. Multiplying Eq. (2.2a) by $P_j(\eta)$ and integrating over η from 0 to 1 gives

$$\sum_n [A_n P_n(\xi_0)-B_n Q_n(\xi_0)+E_0 f \xi_0 \delta_{n1}]X_{jn}=0\,, \tag{2.5}$$

where

$$X_{jn}=\int_0^1 d\eta\, P_j(\eta)P_n(\eta)\,. \tag{2.6}$$

Values of X_{jn} have been tabulated by Berreman.[6] Likewise, from Eq. (2.2b) we find

$$\sum_n [\epsilon A_n P_n'(\xi_0)-B_n Q_n'(\xi_0)+E_0 f \delta_{n1}]X_{jn}=0\,. \tag{2.7}$$

Introducing

$$Y_{jn}\equiv\int_{-1}^0 d\eta\, P_j(\eta)P_n(\eta)=(-1)^{j+n}X_{jn}\,, \tag{2.8}$$

we may rewrite Eqs. (2.2c) and (2.2d) as

$$\sum_n [A_n P_n(\xi_0)-C_n Q_n(\xi_0)+E_1 f \xi_0 \delta_{n1}]Y_{jn}=0\,, \tag{2.9}$$

and

$$\sum_n [A_n P_n'(\xi_0)-C_n Q_n'(\xi_0)+E_1 f \delta_{n1}]Y_{jn}=0\,. \tag{2.10}$$

Since Eqs. (2.2e) and (2.2f) must be true for a continuous range of ξ, it follows that

$$B_n P_n(0)=C_n P_n(0)\,, \tag{2.11}$$

or

$$B_n=C_n,\quad n=0,\,2,\,4,\ldots\,. \tag{2.12}$$

Also

$$B_n P_n'(0)=\epsilon C_n P_n'(0)\,, \tag{2.13}$$

or

$$B_n=\epsilon C_n,\quad n=1,\,3,\,5,\ldots\,. \tag{2.14}$$

Finally the internal electric field E_1 is given by

$$E_1=E_0/\epsilon\,. \tag{2.15}$$

Noting that

$$C_n=\tfrac{1}{2}B_n[1+\epsilon^{-1}+(-1)^n(1-\epsilon^{-1})]\,, \tag{2.16}$$

and

$$X_{jn}+Y_{jn}=\frac{2\delta_{jn}}{2n+1}\,, \tag{2.17}$$

gives

$$\frac{2}{2j+1}A_j P_j(\xi_0)=\sum_n [B_n Q_n(\xi_0)X_{jn}+C_n Q_n(\xi_0)Y_{jn}]-fE_0\xi_0 X_{j1}-E_1 f\xi_0 Y_{j1}\,, \tag{2.18}$$

and

$$\frac{2}{2j+1}A_j P_j'(\xi_0)=\sum_n [B_n\epsilon^{-1}Q_n'(\xi_0)X_{jn}+C_nQ_n'(\xi_0)Y_{jn}]-E_0f\epsilon^{-1}X_{j1}-E_1fY_{j1}\ . \tag{2.19}$$

From Eqs. (2.17), (2.18), and (2.19) we finally obtain

$$\sum_n T_{jn}B_n=R_j\ , \tag{2.20}$$

where

$$T_{jn}=X_{jn}\left\{[Q_n(\xi_0)P_j'(\xi_0)-\epsilon^{-1}Q_n'(\xi_0)P_j(\xi_0)] + \frac{(-1)^{j+n}}{2}[Q_n(\xi_0)P_j'(\xi_0)-Q_n'(\xi_0)P_j(\xi_0)][1+\epsilon^{-1}+(-1)^n(1-\epsilon^{-1})]\right\}\ , \tag{2.21}$$

and

$$R_j=E_0f\xi_0\{P_j'(\xi_0)X_{j1}[1-(-1)^j\epsilon^{-1}]-\tfrac{2}{3}\epsilon^{-1}\delta_{j1}\}\ . \tag{2.22}$$

A formal solution for B_n is obtained in the form

$$B=T^{-1}R\ , \tag{2.23}$$

where T^{-1} denotes the inverse to the T matrix. The coefficients A_j are then given by

$$A_j=\frac{j+\frac{1}{2}}{P_j(\xi_0)}\left\{\sum_n [B_nQ_n(\xi_0)X_{jn}+C_nQ_n(\xi_0)Y_{jn}]-f\xi_0E_0X_{j1}+E_0f\epsilon^{-1}\xi_0(-1)^jX_{j1}\right\}\ , \tag{2.24}$$

where B_n and C_n are given by Eqs. (2.23) and (2.16). The natural oscillations of the system are determined by the condition that a nonzero amplitude exist even when E_0 is zero. From Eqs. (2.20) and (2.22) we see that this means when $R_j=0$ there still will be a nonvanishing set of B_n. Thus, the determinant of T must vanish and

$$\Delta(\omega)\equiv\det T=0\ , \tag{2.25}$$

is the condition for a surface shape resonance. We will denote the roots of this equation by $\omega=\omega_r$.

Having obtained the resonance frequencies, let us now calculate the decay rate for the excitation disappearing into local (energy deposition) excitations. In the case of electronic excitations these are from inelastic electron scattering (resistive losses). In the case of ionic excitations these are low-frequency phonons. In either case the theory will be cast in microscopic language and only the dielectric constant will enter the formulas.

In calculating Eq. (2.25) cognizance must be taken of the fact that ϵ, and hence T, are complex quantities. In principle the ω_r roots are complex numbers. The real part of ω_r is the resonance frequency and the imaginary part is proportional to the decay rate into "local" excitations. Alternatively, if the imaginary part of ϵ is small, one may define the resonance frequencies by the condition

$$\mathrm{Re}\Delta(\omega_r)=0\ . \tag{2.26}$$

Then let us expand $\Delta(\omega)$ around the shape resonance:

$$\Delta(\omega)=\Delta(\omega_r) + (\omega-\omega_r)\frac{\partial\Delta(\omega)}{\partial\omega}\bigg|_{\omega_r}+\cdots\ , \tag{2.27}$$

or

$$\Delta(\omega)\simeq\mathrm{Re}\Delta'(\omega_r)\left\{\omega-\omega_r + i\frac{\mathrm{Im}\Delta(\omega_r)}{\mathrm{Re}\Delta'(\omega_r)}\right\}\ , \tag{2.28}$$

which we may interpret as

$$\Delta(\omega)\sim\omega-\omega_r+\frac{i}{2}\Gamma_e\ , \tag{2.29}$$

where Γ_e is the desired decay rate

$$\Gamma_e=2\frac{\mathrm{Im}\Delta(\omega_r)}{\mathrm{Re}[\partial\Delta(\omega_r)/\partial\omega_r]}\ . \tag{2.30}$$

This result was obtained previously[7] in the context of the optical properties of spheroidal particles.

In the following sections we will need to know the absolute magnitude of the dipole moment of a surface shape resonance. In order to determine this quantity it will be necessary to introduce a normalization condition. This is found by noting that the power delivered to "local" excitations is

$$P_e=\Gamma_e\hbar\omega_r\ , \tag{2.31}$$

where $\hbar\omega_r$ is the energy corresponding to one quantum of bump excitation. The power may be computed from the expression for Joule heating

$$P_e=\frac{\sigma}{2}\int d\vec{r}\,|E|^2\ , \tag{2.32}$$

where σ is the conductivity of the solid and the integral extends over the entire solid. Thus,

$$P_e=\frac{\sigma}{2}\int_{S_1}dS_1\,\frac{\Phi_1^*}{h_{\xi_0}}\frac{\partial\Phi_1}{\partial\xi_0}+\frac{\sigma}{2}\int_{S_2}dS_2\,\frac{\Phi_{\rm III}^*}{h_{\eta_0}}\frac{\partial\Phi_{\rm III}}{\partial\eta_0}\ , \tag{2.33}$$

where we have integrated by parts and employed Laplace's equation. The surfaces S_1 and S_2 are specified by

$$S_1:\ \xi=\xi_0,\ 0<\eta<1,\ 0<\phi<2\pi\ , \tag{2.34a}$$

and

$$S_2:\ \xi_0<\xi<\infty,\ \eta=0,\ 0<\phi<2\pi\ . \tag{2.34b}$$

In Eq. (2.33), h_{ξ_0} and h_{η_0} refer to the standard curvilinear metric coefficients. The surface area elements are $dS_1=h_{\eta_0}h_\phi d\eta d\phi$ and $dS_2=h_{\xi_0}h_\phi d\xi d\phi$. Letting

$$I_{n\nu}\equiv\int_{\xi_0}^{\infty}d\xi\,Q_n(\xi)Q_\nu(\xi)\ , \tag{2.35}$$

we finally obtain, after some simplification,

$$P_e=\sigma\pi f(\xi_0^2-1)\sum_{n\nu}A_n^*A_\nu P_n(\xi_0)P_\nu'(\xi_0)X_{n\nu}+\sigma\pi f\sum_{n\nu}C_n^*C_\nu P_n(0)P_\nu'(0)I_{n\nu}\ . \tag{2.36}$$

Equation (2.36), in conjunction with Eqs. (2.31) and (2.30), will be used as a normalization condition to define the magnitudes of A_n, B_n, and C_n, and of the dipole moment μ.

III. DECAY TO PHOTONS AND SURFACE PLASMONS

We have treated the spheroidal bump on a plane as a dipole oscillating due to natural electronic charge fluctuations in the system. The coupling of the electric dipole above the surface to the delocalized surface-plasmon modes determines part of the decay rate of the localized plasmon mode. Other channels for decay obviously exist, however. One such channel, that of local heating, was taken into account in Sec. II. In this section we study the decay into photons and surface plasmons. The problem of decay into photons has a long history dating back to Sommerfeld's study of a radiating dipole antenna on the earth's surface. More recently, Chance, Prock, and Silbey[8] have studied the radiation properties of a molecule near a surface. We shall apply their formalism to the problem of a bump on a surface without a nearby molecule.

For a dipole oriented perpendicular to the interface the decay rate is given, in the dipole approximation, by

$$\hat{\Gamma}_{\rm rad}(\perp)=q-\tfrac{3}{2}q\,{\rm Im}\int_0^1 R''e^{-2l_1\hat{d}}\frac{u^3du}{l_1}\ , \tag{3.1}$$

where

$$R''=\frac{\epsilon_1 l_2-\epsilon_2 l_1}{\epsilon_1 l_2+\epsilon_2 l_1}\ , \tag{3.2}$$

$$l_j=-i\left[\frac{\epsilon_j}{\epsilon_1}-u^2\right]^{1/2},\quad j=1,2 \tag{3.3}$$

$$\hat{d}=k_1 d,\ \ k_1=\frac{\omega}{c}n_1,\ \ n_1=\sqrt{\epsilon_1}\ , \tag{3.4}$$

and

$$q=\frac{\Gamma_{\rm rad}}{\Gamma_0}\ . \tag{3.5}$$

Here d is the distance of the dipole from the surface, $\vec{k}_1$ is the propagation vector in medium 1, and ϵ_1 and ϵ_2 are the dielectric functions of medium 1 and 2, respectively. The radiative quantum yield of the system, q, is the ratio of the radiative decay rate to the total decay rate of the bump. The hat on $\Gamma_{\rm rad}$ in Eq. (3.1) indicates that the decay rate is normalized to that in the absence of the surface. In our case $\epsilon_1=1$ and $\epsilon_2=\epsilon(\omega)$. Hence $k_1=\omega/c$ and carrying out the integration yields

$$\Gamma_{\rm rad}=\Gamma_{\rm rad}^{\rm free}\left[1+\tfrac{3}{2}\int_0^{\pi/2}d\theta\,\frac{\sin^3\theta}{(\epsilon-1)[(\epsilon+1)\cos^2\theta-1]}\{[(\epsilon^2+1)\cos^2\theta+(\epsilon-1)]\cos(2k_1 d\cos\theta)+2\epsilon\cos\theta(\sin^2\theta-\epsilon)^{1/2}\sin(2k_1 d\cos\theta)\}\right]. \tag{3.6}$$

From the classical theory of radiation, the free radiative decay rate is

$$\Gamma_{\rm rad}^{\rm free}=\frac{|\mu|^2\omega^3}{3c^3}. \tag{3.7}$$

Combining Eqs. (3.6) and (3.7) and employing atomic units ($e=\hbar=m=1$), we find

$$\Gamma_{\rm rad}=\frac{|\mu|^2\omega^3}{3c^3}\left\{1+\tfrac{3}{2}\int_0^{\pi/2}d\theta\,\frac{\sin^3\theta}{(\epsilon-1)[(\epsilon+1)\cos^2\theta-1]}\left[[(\epsilon^2+1)\cos^2\theta+\epsilon-1]\cos\left[\frac{2\omega}{c}d\cos\theta\right]+2\epsilon\cos\theta(\sin^2\theta-\epsilon)^{1/2}\sin\left[\frac{2\omega}{c}d\cos\theta\right]\right]\right\}. \tag{3.8}$$

At small distances, i.e., $k_1 d<<1$, we write Eq. (3.8) approximately as

$$\Gamma_{\rm rad}=\frac{1}{3}\frac{|\mu|^2\omega^3}{c^3}\left[1+\tfrac{3}{2}\int_0^{\pi/2}d\theta\,\frac{\sin^3\theta}{(\epsilon-1)[(\epsilon+1)\cos^2\theta-1]}[(\epsilon^2+1)\cos^2\theta+\epsilon-1]\right]. \tag{3.9}$$

The integral is evaluated by numerical quadrature.

We now turn to the evaluation of the decay rate into surface plasmons. As we mentioned earlier, the degeneracy of the frequency ω_r with some surface-plasmon frequency allows a decay channel to open which damps out the local bump excitations. The natural way to proceed is to write down the surface-plasmon fields in quantized form, and then couple them to the oscillations of the bump, represented by the dipole moment μ, perpendicular to the surface. This dipole is responsible for "radiation" of surface plasmons along the surface. In order to write down the surface-plasmon fields, one may compare the classical and quantum-mechanical powers dissipated due to the coupling of an oscillating charge to a surface plasmon. Calculations of the coupling constants in the electrostatic limit have been given in the literature.[9] A calculation including the effects of retardation has been given for the special case of an electron gas.[10] The general expression for the coupling constant γ_k appearing in the quantized electric field expression

$$E_x=\sum_k \gamma_k a_k\exp(ikx)+\text{c.c.}, \tag{3.10}$$

where a_k is an annihilation operator, is

$$|\gamma_k|=\left[\frac{4\pi\hbar k}{A}[f_s\epsilon_s'(-\epsilon_s)^{-1/2}+(1-\epsilon_s)(kc)^{-1}\times(-1-\epsilon_s)^{1/2}]\right]^{-1}, \tag{3.11}$$

where A is the surface area, $f_s=(\epsilon_s-1)/2\epsilon_s$, and $\epsilon_s=k^2[(\omega_s/c)^2-k^2]^{-1}$. However, a more general derivation of the power emitted and the decay rate into surface plasmons by a dipole oriented perpendicular to the surface has been given by Philpott.[11] A classical derivation of the same result is also in existence in the literature.[12] It involves only the dielectric function of the protrusion plane system and may be applied to more general situations involving ionic excitations or many-body effects. Here we use the expression for the sought after decay rate from Ref. 11. Thus

$$\Gamma_{\rm sp}=\frac{4\pi|\mu|^2}{\hbar}\left[\frac{\omega_s}{c}\right]^3\frac{(-\epsilon_s)^3}{(-\epsilon_s-1)^{5/2}(1-\epsilon_s)}, \tag{3.12}$$

where we have set ω_s equal to the frequency of the

surface shape resonance.

Equation (3.12) represents the desired result—an expression for the decay rate of the localized excitation into delocalized surface plasmons. It may be calculated in absolute terms since an expression for μ has already been given [see Eq. (2.4)].

IV. RESULTS AND DISCUSSION

In the previous sections we have derived formulas for the frequency of a surface shape resonance and for its decay rate into various excitations of interest. Before stating the results and discussing them, let us consider the calculational procedure.

In our calculations we restricted our attention to the case where Imϵ was sufficiently small to allow it to be treated as a perturbation parameter. This assumption is somewhat restrictive but is valid for some metals, e.g., Ag, at optical frequencies. The restriction may be lifted in a straightforward manner, however.

The eigenfrequencies are determined as roots of the determinant of the T matrix defined by Eq. (2.21). In principle, the T matrix is of infinite dimension. In practice one truncates the size of the matrix and checks for convergence of the roots as the size is increased. The low-lying frequencies converge rapidly while the higher frequencies converge more slowly. A ten by ten matrix was used in this numerical work. In determining the T matrix only the real part of ϵ was used.

The eigenvectors of the T matrix [see Eq. (2.20) with $R_j=0$] were obtained by solving the appropriate set of linear equations and imposing the normalization condition defined by Eqs. (2.30), (2.31), and (2.36). Use was made of the following expansion for the determinant of the T matrix for small Imϵ:

$$\det T \simeq (\det T_1)\left[1-i\frac{\epsilon_2}{\epsilon_1}\mathrm{Tr}(T_1^{-1}G)\right], \tag{4.1}$$

where T_1 is the T matrix defined with real ϵ and

$$G_{jn}\equiv X_{jn}\{-Q_n'(\xi_0)P_j(\xi_0)+\tfrac{1}{2}(-1)^{j+n}[Q_n(\xi_0)P_j'(\xi_0) -Q_n'(\xi_0)P_j(\xi_0)][1-(-1)^n]\}\ . \tag{4.2}$$

The calculations reported here are for silver protrusions sticking out of a silver metal half-space. We will not be concerned with how the surface shape resonance is excited, although a number of methods come to mind. One is through the use of optical radiation impinging on the surface. Another is through the use of an incident electron or ion beam. The excitation of the resonance may readily be monitored through the secondary radiation that is produced. In the case of charged projectiles it may also be seen in the electron energy-loss spectrum.

One way of characterizing the shape resonance is through the value of the real part of the dielectric constant at the resonance frequency. In Table I the low-lying azimuthally symmetric shape resonances are studied as a function of the aspect ratio of the bump, a/b. The lowest-lying resonance occurs at a dielectric constant given by ϵ_r^0. The first-excited state occurs at ϵ_r^1 and the second-excited state (which is azimuthally symmetric) occurs at ϵ_r^2. The excited states correspond to excitations with nodes of potential on the solid's surface while the ground state is nodeless. The general trend is for ϵ to get more negative as the aspect ratio is increased. This is in qualitative agreement with previous studies of isolated spheroids. The magnitude of ϵ, however, is less than that of the corresponding isolated spheroid with the same aspect ratio. It should be emphasized that the numbers presented in Table I are universal numbers, valid for any metal or dielectric.

The numbers in Table I are translated into frequencies by using the optical data of the material of interest. For Ag the optical constants of Johnson and Christy[13] were used to obtain the resonance frequencies.

In Fig. 2 a plot is made of the resonant frequency as a function of aspect ratio for fixed a ($a=200a_0$). Two curves are shown: one for the ground state and one for the first-excited state.

TABLE I. Dielectric constant of surface shape resonances as a function of aspect ratio of bump.

a/b	ϵ_r^0	ϵ_r^1	ϵ_r^2
1.2	−4.29	−1.80	−1.36
1.5	−5.64	−2.85	−1.80
1.8	−6.64	−2.86	−1.92
2.0	−7.35	−2.97	−2.04
2.5	−9.25	−3.30	−2.33
3.0	−11.3	−3.72	−2.61
3.5	−13.6	−4.20	−2.89
4.0	−15.9	−4.75	−3.18

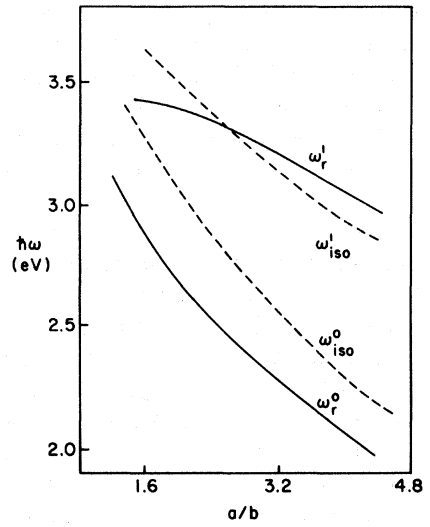

FIG. 2. Resonance energy as a function of the spheroid aspect ratio, both for a hemispheroidal protrusion from a smooth surface and for an isolated spheroid. The ground states are labeled ω_r^0 and ω_{iso}^0, respectively, for the hemispheroidal protrusion and the isolated spheroid. The corresponding first excited states are labeled ω_r^1 and ω_{iso}^1. The curves are for silver.

The data is for silver. As the aspect ratio is increased in magnitude the frequencies of the excitations fall off. The same figure shows the resonance frequency for both the dipole and quadrupole resonance of isolated silver spheroid.

Figure 3 shows the magnitude of the dipole moment of the system as a function of the aspect ratio a/b for fixed a ($a=200a_0$). The upper curve is for the ground state and the lower curve is for the first-excited state. It should be noted that the size of the electric dipole moment is very large. This follows from a comparison of the classical and quantum expressions for dipole moments and dipole transition moments. In classical electro-

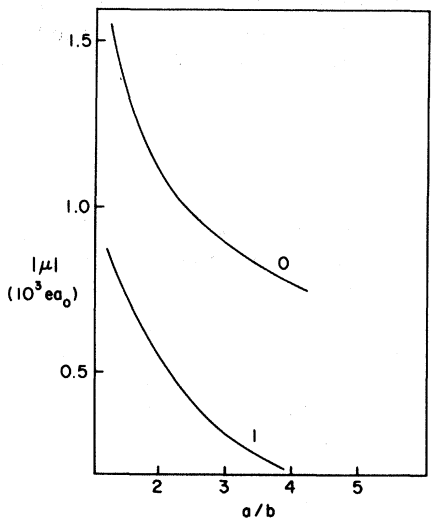

FIG. 3. Magnitude of the electric dipole moment as a function of the aspect ratio for a given value of a. The ground state is labeled (0) and the first-excited state (1).

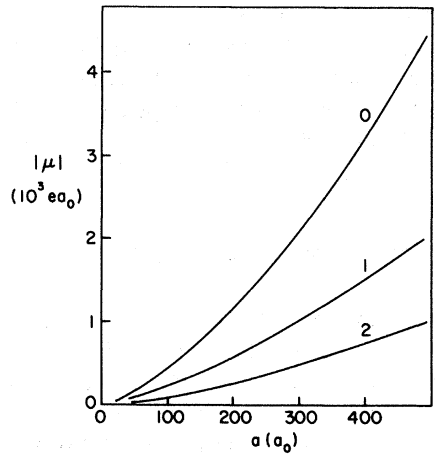

FIG. 4. Magnitude of the electric dipole moment as a function of semimajor axis a for fixed aspect ratio. Data for the three most low-lying states are shown [labeled (0), (1), and (2)]. Here $a/b=2.0$. The resonance energies are 2.71, 3.39, and 3.62 eV, respectively. The dielectric constants are from Ref. 13.

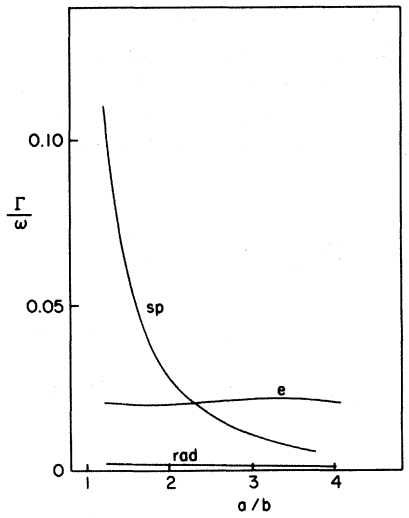

FIG. 5. Ratio of decay rate to resonance frequency for three branches of decay: e stands for inelastic electron scattering, sp stands for surface-plasmon decay, and rad stands for photon decay. The data is plotted as a function of aspect ratio.

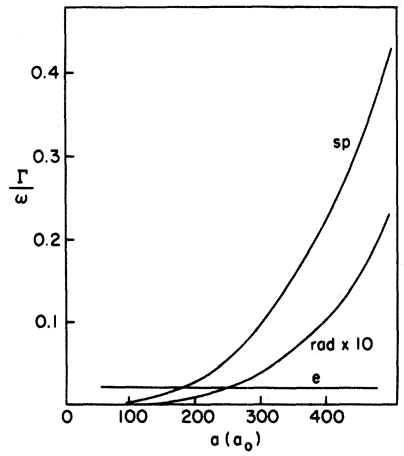

FIG. 6. Same as Fig. 5 but plotted as a function of semimajor axis size a. Note that Γ_{rad}/ω_r^0 is magnified by a factor of 10. Here $a/b=2.0$ and the resonance frequency for the lowest state is 2.71 eV.

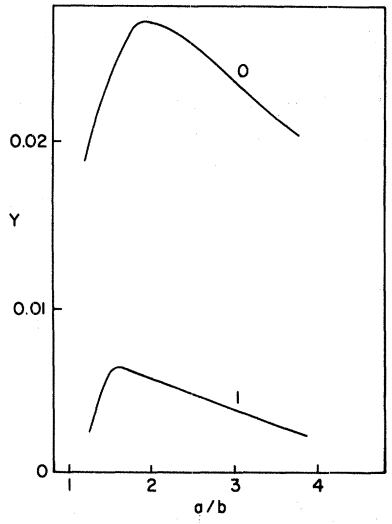

FIG. 8. Radiative yield vs aspect ratio for fixed a.

dynamics the polarizability of an object is proportional to its volume. Thus, for example, for a sphere $\alpha \sim a^3$, where a is the radius. In the quantum-mechanical expression for α one has a sum of terms of the form $\alpha \sim \mu^2/\Delta\omega$, where $\Delta\omega$ is a frequency difference. Simply equating these expressions and letting $a=200a_0$, $\hbar\Delta\omega=3$ eV gives $\mu \sim 10^3 e a_0$, in agreement with the calculated magnitude.

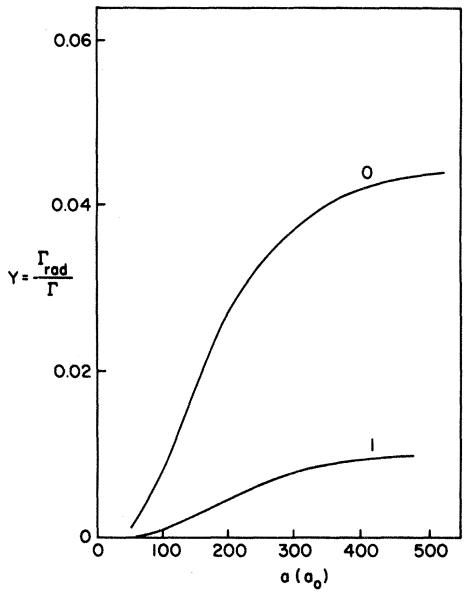

FIG. 7. Radiative yield as a function of semimajor axis for the ground (0) and first-excited states (1). Here $a/b=2.0$. The resonance energies are 2.71 eV ($\hbar\omega_r^0$) and 3.39 eV ($\hbar\omega_r^1$).

Figure 4 shows the strength of the dipole growing as a function of axis size for fixed aspect ratio. The three curves correspond to the three most low-lying states. As the size of the bump increases, one expects an increase in μ according to the arguments just given. The ground state, being nodeless, would be expected to have the largest dipole. The presence of nodes in the excited states causes some degree of cancellation with a subsequent reduction in dipole strength.

An examination of Fig. 4 shows the scaling behavior $\mu \sim a^{1.5}$. Since the aspect ratio is fixed, this also implies $\mu \sim f^{1.5}$. From Eqs. (2.31) and (2.36) it follows that the coefficients A_n and B_n scale as $f^{-0.5}$. Equation (2.16) implies a similar scaling for C_n, so from Eq. (2.4) we find $\mu \sim f^{1.5}$.

In Fig. 5 we consider the various damping rates, expressed in units of the resonance frequency, for the ground-state surface shape resonance, as a function of aspect ratio for fixed $a=200a_0$. As the aspect ratio increases the decay rate to frequency ratio for electron collisions remains fairly constant while that for surface plasmons or photons falls off.

Figure 6 gives the same ratios as in Fig. 5, but plotted as a function of the axis a for fixed aspect ratio ($a/b=2$). It is seen that the radiation into surface plasmons and photons grows substantially with size, whereas the electron-hole rate remains constant. For large sizes ($a \gtrsim 200a_0$), the long-range energy deposition mechanisms dominate over the electron-scattering mechanism and are the

main source of the limited Q of the resonance.

Figure 7 shows a plot of the radiative yield of the ground and first-excited state shape resonances as a function of size for fixed aspect ratio. As one might expect, the radiative yield grows with increasing size. Figure 8 shows the same yield as a function of aspect ratio for fixed $a = 200a_0$. The falloff with increasing a/b is probably due to the reduction in the volume of the bump, and hence of the dipole moment.

In conclusion we have shown that a surface with a protrusion possesses a set of shape resonances whose frequencies and damping rates are determined solely by the geometric and dielectric properties of the system.

ACKNOWLEDGMENTS

Helpful discussions with Doctor S. Garoff, Doctor A. Genack, Doctor A. Nitzan, and Doctor D. Weitz are appreciated.

[1] *Surface Enhanced Raman Scattering,* edited by R. K. Chang and T. E. Furtak (Plenum, New York, 1981).
[2] D. A. Weitz, S. Garoff, C. D. Hanson, T. J. Gramila, and J. I. Gersten, Opt. Lett. 7, 89 (1982).
[3] C. K. Chen, A. R. B. deCastro, and Y. R. Shen, Phys. Rev. Lett. 46, 145 (1981).
[4] D. W. Berreman, Phys. Rev. 163, 855 (1967).
[5] R. Ruppin, Solid State Commun. 39, 908 (1981).
[6] W. H. Weber and G. W. Ford, Phys. Rev. Lett. 44, 1774 (1980).
[7] J. I. Gersten and A. Nitzan, J. Chem. Phys. 75, 1139 (1981).
[8] R. R. Chance, A. Prock, and R. Silbey, in *Advances in Chemical Physics,* edited by I. Prigonine and S. Rice (Wiley, New York, 1978), Vol. 37.
[9] J. I. Gersten, Phys. Rev. 188, 774 (1969).
[10] J. M. Elson and R. H. Ritchie, Phys. Rev. B 4, 4129 (1971).
[11] M. R. Philpott, J. Chem. Phys. 62, 1812 (1975).
[12] H. Morawitz and M. R. Philpott, Phys. Rev. B 10, 4563 (1974).
[13] P. B. Johnson and R. W. Christy, Phys. Rev. B 6, 4370 (1972).